ISO Observations of the 53W002 Group at 6.7μm: In Search of the Oldest Stellar Populations at $z = 2.4$ [1]

William C. Keel[2] and Wentao Wu[3]

Department of Physics and Astronomy, University of Alabama, Box 8709324, Tuscaloosa, AL 35487-0324; keel@bildad.astr.ua.edu

Paul P. van der Werf

Sterrewacht Leiden, Postbus 9513, 2300 RA Leiden, The Netherlands; pvdwerf@strw.leidenuniv.nl

Rogier A. Windhorst

Dept. of Physics and Astronomy, Arizona State University, Box 1504, Tempe, AZ 85287; Rogier.Windhorst@asu.edu

James S. Dunlop

Royal Observatory Edinburgh, Blackford Hill, Edinburgh EH9 3HJ, UK; J.Dunlop@roe.ac.uk

Stephen A. Eales

Department of Physics and Astronomy, University of Wales, Cardiff, 5, The Parade, Cardiff CF24 3YB, UK; Steve.Eales@astro.cf.ac.uk

Ian Waddington

Astronomy Centre, Dept. of Physics & Astronomy, University of Sussex, Falmer, Brighton BN1 9QH, U.K.; I.Waddington@sussex.ac.uk

---

[1]Based on observations with ISO, an ESA project with instruments funded by ESA Member States (especially the PI countries: France, Germany, the Netherlands and the United Kingdom) and with the participation of ISAS and NASA.

Martha Holmes[4]

Dept. of Physics and Astronomy, Box 1803-B, Vanderbilt University, Nashville, TN 37235;

martha.j.holmes@vanderbilt.edu

Received ______________; accepted ______________

Submitted to PASP

[2]Visiting Astronomer at the Infrared Telescope Facility, which is operated by the University of Hawaii under Cooperative Agreement no. NCC 5-538 with the National Aeronautics and Space Administration, Office of Space Science, Planetary Astronomy Program.

[3]Present address: Department of Astronomy & Astrophysics, 525 Davey Lab, Pennsylvania State University, University Park, PA 16802

[4]NSF Research Experiences for Undergraduates participant at the University of Alabama

ABSTRACT

We present a deep ISO observation at 6.7μm of the 53W002 group of galaxies and AGN at $z = 2.4$. This approximately samples the emitted K band. The faint, blue star-forming objects are not detected, as expected from their very blue color across the emitted optical and UV. However, 53W002 itself is detected at the $\approx 3\sigma$ level, with an emitted $V - K$ color appropriate for a population formed starting at $z = 3.6$–7.0 with most likely value $z = 4.7$. This fits with shorter-wavelength data suggesting that the more massive members of this group, which may all host AGN, began star formation earlier in deeper potential wells than the compact Lyman α emission objects. Two foreground galaxies are detected, as well as several stars. One additional 6.7μm source closely coincides with an optically faint galaxy, potentially at $z = 2 - 3$. The overall source counts are consistent (within the errors of such a small sample) with the other ISO deep fields at 6.7μm.

Subject headings: galaxies: high-redshift – galaxies: evolution – infrared: galaxies

1. Introduction

As our understanding of galaxies at high redshifts improves, it becomes important to be able to compare them in increasing detail with nearby systems, as well as with evolutionary models. This has driven a number of studies of these objects in the infrared to sample the emitted optical range with its many diagnostic spectral features for accessible redshifts. Near-infrared spectroscopy has revealed the locally well-studied [O III], [N II], and Balmer emission lines, and in a few cases spectral breaks that indicate an age for the dominant stellar population (Eales & Rawlings 1993, Pettini et al. 1998, 2001, Teplitz et al. 2000, Motohara et al. 2001). Multiband photometry has provided important information as well, especially given the difficulty of obtaining spectra of such faint objects against the high background of ground-based observations.

Long wavelength baselines improve estimates of the spectral shape, and consequently effective ages, of stellar populations, since the sensitivity to a minority population of young stars and to dust effects are both reduced. We present here deep ISO observations of a group of objects at $z = 2.4$, corresponding to 2μm in the emitted frame, and thus offering a sensitive probe of the oldest stellar populations in these objects. At high redshifts, even crude limits on age of a stellar population become very sensitive measures of formation time, and can sometimes limit cosmological parameters, as the redshift/age relation becomes stronger (Stockton et al. 1995, Dunlop et al. 1996, Spinrad et al. 1997).

We targeted the region around the radio galaxy 53W002 at $z = 2.39$ (Windhorst et al. 1991) for ISO observations in the emitted near-infrared. This system has been found to be part of a grouping or cluster extending over at least 7' (3.5 Mpc for the WMAP cosmology with $H_0 = 71$ km s^{-1} Mpc^{-1}, $\Omega_M = 0.27$, and Λ-dominated flat geometry), including 5 additional AGN and 8 star-forming objects detected through narrow Lyman α emission (Pascarelle et al. 1996, Keel et al. 1999). These fainter Lyman α sources are

especially interesting as candidate protogalactic objects (of rather low mass). They are quite small, with effective radii in the emitted ultraviolet of $0\farcs1$–$0\farcs2$ (1–2 kpc), and some are so closely paired as to suggest a short timescale against merging, as expected from hierarchical scenarios. This field offered the chance for uniquely deep detections or limits on such objects, since we could observe 7 such objects at once and derive an average flux or limit several times deeper than possible for an individual target. While it was clear that detections of young blue populations would be at the very limit of ISOCAM's sensitivity, the opportunity to measure so many high-redshift targets (both AGN and star-forming systems) at once was quite attractive.

More recent NICMOS observations (Keel et al. 2002) show that the star-forming objects are very blue (and presumably thus quite poor in both dust and metals), so that their detections at 6.7μm would be unlikely. Still, these data are valuable in setting an explicit limit on the emitted $R-K$ colors, and in the likely detection of 53W002 itself. This is also one of the handful of deepest ISO images at this wavelength, in a field for which supporting data from the optical, near-IR, and radio regimes are available, so the source counts and identifications are of interest in themselves. For low-redshift galaxies, this wavelength falls between photospheric starlight and the hottest dust emission, making the detected population relatively sensitive to high-redshift galaxies.

2. Observations

2.1. ISO 6.7μm Data

The 53W002 field was observed with ISOCAM (Cesarsky et al. 1996) on orbits 500 and 521. The LW2 filter, with half-power transmission points at 5.0 and 8.5 μm and effective wavelength 6.7 μm for a flat spectrum, was used to approximate the emitted K

band at $z = 2.4$ (the effective emitted-frame wavelength actually corresponds to 1.97μm). Since we were interested in 11 objects in the 53W002 group (including three foreground and background Lyman α emitters at $z = 2.05 - 2.7$), a tradeoff had to be made between covering a wide enough field and high point-source sensitivity. We used the 3” pixel scale, undersampling the LW2 PSF in the interest of covering a larger region at once. The final spatial resolution will be somewhat worse than this, since data from many offset pointings are stacked. Two levels of pointing offsets were used for these data. At each of 21 positions, 3×3 sets of 10×10.08-second exposures were done, with the 3×3 pattern using offsets of 5 pixels (15”). A set of 21 of these pointings was laid out to cover the area spanning most of the known objects around 53W002, with 45” spacing in both celestial coordinates. To provide scheduling flexibility while assuring that the right regions were observed, these locations were specified in celestial rather than spacecraft coordinates, with the result that the detector orientation is skewed to the pointing grid (by about 109° for orbit 500 and 129° for orbit 521, with rotations of 0.25° or less within each orbit). The overlap of these observations is shown in Fig. 1. To minimize the time used in microslews between these positions, they were observed in a boustrophedonic order. For clarity in describing the reductions, we will refer to each 3×3 set of exposures as a raster.

Before each raster observation, a brief exposure was made using the LW1 filter, taking advantage of experience which suggested that the LW detector response to transients could be improved by a change in the background level. The total exposure time in LW2 was 19051 seconds (5.3 hours), of which a typical useful total at a given sky position is 13000 seconds in the inner part of the field. The region of best exposure is roughly circular with a radius of 90”, centered at (J2000) α = 17:14:13.0, δ = +50:15:57. There is considerable structure at the 10% level in the exposure pattern even within this region, but this amplitude does not strongly change the detection limit. In comparison to other ISO surveys at this wavelength, this study is thus substantially deeper than the CFRS field examined

by Flores et al. (1999), comparable in exposure to the LW2 data on the Hubble Deep Field presented by Serjeant et al. (1997) and about 3 times shorter than the very deep SSA13 and Lockman Hole observations by Taniguchi et al. (2002).

Reduction of these data began using the ISOCAM CIA package (v4.0, April 2000 release, described in Delaney 2000). Its routines were used to clean the data stream of incomplete and otherwise invalid exposures, correct for the dark pattern by standard library frames, deglitch, and stabilize the individual exposures. Deglitching, which corrects for long-lasting radiation-induced events, was found to be most effective with the multiresolution median algorithm in CIA. The stabilization step corrects for the substantial time constant of the detector in responding to a change in illumination (such as happens at each change of pointing). The data for each raster were combined to form a single mosaic, rejecting pixels masked as uncorrectable in the earlier stage, and each mosaic was projected onto a common celestial-coordinate frame, expanded to $1''\!.0$ pixels using the C routine *project* distributed with the CIA package. This expansion preserved the intensity-flux calibration in mJy per solid angle. The number of glitches not rejected by these techniques was still substantial, so we carried out further processing and masking using the `combine` and `imedit` tasks within IRAF.

Residual flat-field structures were apparent in the raster products, so these were corrected using a median frame for each orbit's data. Drifts in background level between rasters were also removed. Glitches that remained after the CIA processing were identified by comparison of spatially overlapping rasters, and masked before combining. The best results were found by masking the outer parts of each raster as well, leaving those regions which were included in at least 6 of the 9 constituent observations (a region 111" square in each case). The final data mosaic combined all these masked raster products with 3σ rejection. The effective resolution of this mosaic should be slightly better than 6" FWHM,

a combination of the input 3" pixel scale and stacking of variously offset observations. This value varies significantly depending on a source's exact location with respect to the observed pixel grid; some star images have a FWHM as small as 4".

The mosaicked image still shows residual variations in blank-sky level, associated with slight slope changes from one observation to the next. We removed these using a running 11×11-arcsecond median filter, which substantially improved the image uniformity and reliability of aperture fluxes while not altering image structure on relevant scales for our small targets. The detection threshold was assessed through statistics of individual pixel values, and by the statistics of detected positive and negative peaks after smoothing by a Gaussian effective PSF with 5-arcsecond FWHM. Nine ISO sources are robust to the details of selection aperture and measuring radius within the 4–8" range, and to whether single discrepant pixels are rejected or not. The effective 3σ flux limit across the central high-exposure area is about 0.027 mJy, below which the non-Gaussian noise distribution prevents us from saying anything useful about the number of sources. We also estimated the mean noise by photometry with the same 5" radius on a set of (blank) positions derived from the object locations by 10–20" offsets in each coordinate. The mean 1σ error found in this way is 0.010 mJy, in good agreement with the estimate from statistics of positive and negative fluctuations.

The nominal astrometric positioning of ISOCAM frames is known to change with motions of the lens wheel (Blommaert et al. 2001), typically by 2-3 pixels. The only independent way for us to check the coordinate system is through the bright interacting galaxy 53W003 at $z \simeq 0.05$, near the north edge of the mosaic. The best match between its optical and mid-IR structures comes for a 6" shift in each coordinate, such that the actual coordinates of an object fall SE of the values given by the nominal ISOCAM pointing. This offset also aligns two much fainter sources with relatively bright red stars, and two known

galaxies with their optical locations, so we adopt this astrometric location. The mean offsets, in the sense of corrections to be applied to the nominal ISO header coordinates, are $\Delta\alpha = +0.62^s$, $\Delta\delta = -5.4''$, which have been applied to the listed source positions. The possibility remains of a systematic shift between the two orbits' data, which we can limit by noting that substacks of the region of 53W002 itself, where the two data sets overlap, both recover consistent positions of ISO sources (within the limits set by their flux levels). Any differential offset between the two sets is too small to be detected with such a faint target. This also limits any possible offsets associated with lens-wheel rotations which accompanied some of the interspersed LW1 "reset" exposures.

We carried out tests for the reality of possible sources in this field at various stages in the processing, because of the large number of transient events and the availability of many redundant measurements at most locations of interest. Possible bright sources were examined in each raster including their locations, and any interfering glitches were masked before further combination of the rasters. The sources remaining in the final mosaic image (Fig. 2) pass these straightforward tests. For 53W002 itself, we examined various subsets of the data, none of which shows any problem that could in itself mimic a source detection.

For evaluating source counts, the most conservative interpretation is that the LW2 sources with plausible optical, radio, or submillimeter counterparts are real, and an upper bound is that all the statistically significant ($> 3\sigma$) sources are real. Given the behavior of the detectors and radiation environment, it is hard to pin them down more tightly, so we will consider both extremes in counting the overall source population.

The list of detected sources is given in Table 1. Only three bright sources are listed from outside the 90" radius of full exposure; 53W003, a red star, and one additional possible star (object 2), listed at the top of the table. The remainder are from the central area of deep exposure, and form a 3σ cut, as determined by taking the strongest peaks after

convolution with a Gaussian function of 5" FWHM. One source is a good match for the position of a moderate-redshift spiral galaxy, within the WFPC2 frames of Pascarelle et al. (1996).

The ISO detectors' gain varied with such factors as the history of energetic particle flux. Accordingly, we have checked the flux calibration for consistency with stellar atmosphere models, as was done by the HDF-South survey as well (Oliver et al. 2002). In this case, we used catalogs of stellar magnitudes from B through K, taken from images at Palomar (Neuschaefer & Windhorst 1995), Kitt Peak (Keel et al. 1999), and the NASA Infrared Telescope Facility (section 2.2). These were supplemented by B and R magnitudes from the USNO A-2 catalog of the Palomar Sky Survey (Monet 1998, Monet et al. 2001) for the brightest stars, which were saturated in the deep CCD images. The optical and near-IR fluxes were used to predict a flux at 6.7μm for comparison with the derived ISO values. Nondetections are important as well as detections, verifying the detection threshold. Rare stars with dust shells will appear too bright in the mid-IR compared to the photospheric prediction, but for a group of stars this should not change the derived flux limit. As it happened, the red star to the NE of 53W002 (number 6 in Table 1 and Fig. 3) was especially important, having a color-derived spectral type of M2 V. The stellar data are consistent with the nominal ISO LW2 flux scale, so we had no need for any correction and adopt source fluxes "as is". This comparison limits any systematic variation in the ISO flux scale to the $\pm30\%$ level.

2.2. Supporting Data

We have made use of previously reported data from the ground and space, including WFPC2 images from Pascarelle et al. (1996, 1998), NICMOS images in F110W and F160W filters at 1.1 and 1.6μm (Keel et al. 2002), wide-field optical B and V imagery from the

KPNO 4-m prime-focus camera (Keel et al. 1999), and deep K and narrowband (redshifted Hα) imagery of the immediate environs of 53W002 (Keel et al. 2002).

An additional, shallower K-band mosaic of the entire full-exposure ISO field was obtained during one of the same NASA IRTF observing sessions. The NSFCam system was used at $0''.3$ per pixel, for a typical exposure of 540 seconds for regions outside the deep central observations. The region was covered with nine 3×3 subrasters using 12" offsets. In many cases, the overlap regions of these subrasters do not include bright enough objects to register them from the K data, so we stacked the images using relative astrometry from optical KPNO CCD images. The intensity scale was set from observations of UKIRT faint standard stars (Hawarden et al. 2001).

A collective mean-flux limit was set to the submillimeter brightness of the compact objects in the 53W002 grouping, by coadding the archival SCUBA data, as discussed in section 3.3.

3. Members of the 53W002 Group or Cluster

3.1. The radio galaxy 53W002

The ISO data suggest a detection of the radio galaxy 53W002 itself at the $\approx 3\sigma$ level. Depending on the aperture size and details of background subtraction, the derived flux is 0.024–0.039 mJy or $F_\lambda = (2.1 \pm 0.5) \times 10^{-19}$ erg cm^{-2} s^{-1} Å^{-1}. We include a term for error due to "sky" fluctuations as evaluated in section 2.1, added in quadrature. This is slightly conservative, in the sense that the error range 0.024–0.039 mJy includes some of the effects of noise in the sky annulus. Thus, we adopt a measurement of $F_\lambda = (2.1 \pm 0.8) \times 10^{-19}$ erg cm^{-2} s^{-1} Å^{-1}. This furnishes a constraint on the continuum slope, and therefore age, of the dominant stellar population. The central AGN contributes a significant amount of light at

shorter wavelengths, both in emission lines and from its continuum, which can be estimated from spectroscopy and HST image analysis. Concentrating on the longer wavelengths which are less affected by the most recent star-forming history, we adopt starlight fractions of 0.77 at F110W, 0.62 at F160W, and 0.78 in K (from PSF fitting in WFPC2 and NICMOS images by Windhorst et al. 1998 and Keel et al. 2002, and consistent with the spectroscopic estimate of an optical spectral index $\alpha \approx 0.8$ for the AGN by Windhorst et al. 1991). This correction is small enough not to add to the color error, dominated by the ISO point. The starlight flux gives a ratio in F_λ of 5.4 ± 2.8 between emitted wavelengths of 0.65 and 1.97μm. This translates to emitted $R - K = 2.3 \pm 0.4$, or, adding the flat continuum shape from Keel et al. (2002), $V - K = 3.2 \pm 0.4$.

The emission-line equivalent widths, and image decomposition of the HST data, indicate that light from the active nucleus is a significant contributor in the emitted-frame ultraviolet and optical bands (Windhorst et al. 1991; Windhorst, Keel & Pascarelle 1998). We thus examine whether either the AGN contribution (perhaps reddened) might contribute to the observed ISO flux. Line emission should contribute only a small fraction of the ISO detection, based on scaling from the observed Lyman α, Hα, and [O III] emission. At $z = 2.4$, the response of the LW2 filter extends from 1.47–2.50μm at half-peak transmission. This band contains spectral features including Paschen α at 1.87μm, as well as Br γ at 2.16μm and the adjacent H_2 S(1) line, which is comparably strong in some galaxy contexts. Using the constants in Osterbrock (1989, Table 4.4), for low densities at 10^4 K, the theoretical ratios to Hα are 0.12 for Paschen α and 0.03 for Brackett γ. The IRTF data in Keel et al. (2002) give a total intensity for Hα (including some contribution from [N II]) of 1.7×10^{-15} erg cm^{-2} s^{-1}. To convert the prediction from scaling based on Hα intensity to an in-band LW2 flux, we take a simple trapezoidal approximation to the passband shape, giving an approximate detected flux of 2.0×10^{-15}erg cm^{-2}s^{-1} in the LW2 passband. Of this, the strong hydrogen recombination lines would contribute at most about

15%, so that within these error bars we can safely neglect this correction.

There is a foreground elliptical galaxy at $z \approx 0.6$ appearing about 7" NW of 53W002, potentially confusing the detection of 53W002. This is the galaxy numbered 6 by Windhorst et al. (1991, 1994), not to be confused with object 6 of Pascarelle et al. (1996) and later papers (which is 53W002 itself). We considered whether blending with this object might increase the measured flux of 53W002 in the ISO data, but its effect must be unimportant for two reasons. The statistics of the data stack allow the possibility of two sources at such a separation, but this would be inconsistent with the astrometry of other sources nearby. In particular, the stellar identification to the NW of 53W002 would become a blank field. This is important because this object is so close that it would share whatever detailed pointing errors apply to the area around 53W002 itself. The star image is close to the expected PSF for a point source, which implies that 53W002 (located 85" away) did not suffer pointing errors between rasters which could degrade the image size. Furthermore, the LW2 passband falls well on the long-wavelength side of the stellar emission for even old populations at moderate redshifts; we see this galaxy near 4.2μm in its emitted frame, so the predicted flux is a small fraction of the observed value for 53W002.

Fig. 4 shows the broadband photometry of 53W002 compared to population synthesis models from Worthey (1994) for ages 1.0–2.0 Gyr, after allowance made for the contribution of the central AGN following Windhorst et al. (1998) and Keel et al. (2002). Normalized to the near-IR points that span the emitted optical range 4700–6600 Å , these models indicate that the error range on the ISO measurements spans the range 0.8–2.1 Gyr in single-burst age, with the error range centered near 1.5 Gyr. These values indicate a "formation redshift" for the onset of widespread star formation $z_f = 3.6 - 7.7$, with the error range centered at $z_f = 4.7$. We neglect reddening and any contribution of the AGN at 6.7μm deliberately, to get a maximum possible stellar age. Even this measurement, of quite

modest precision, narrows the epoch of widespread star formation in 53W002 to the redshift range oevr which galaxies are now detected. Age estimates from mid-IR data should be more robust than estimates from shorter-wavelengths, which suffer from the bias toward the youngest populations as observed in the emitted ultraviolet, and the potential role of dust associated with the molecular gas (Scoville et al. 1997). Whether this advantage is realized in practice depends on the accuracy of the mid-IR data. We note as well that there is lingering uncertainty over the near-IR role of AGB stars in the 0.2-2 Gyr age range (as highlighted by Maraston 2004), for which synthesis libraries are still poor in empirical tests.

Significant star formation in 53W002 took place over a span of at least 1 Gyr. The emitted-optical spectrum from Motohara et al. (2001) shows a substantial Balmer jump, indicating a stellar population less than about 5×10^8 years old; a more complete, self-consistent model would be usefully constrained only by much smaller errors in the mid-IR data (as expected from forthcoming *Spitzer* results). Thus we find that the stars in 53W002 were formed over the cosmically brief but dynamically significant span of 1–2 Gyr. In keeping with the general picture of more massive objects beginning star formation first and being able to bind their own enriched gas, 53W002 was the first luminous system to begin star formation in this group, in contrast to the lower-luminosity Lyman α emitters (section 3.3).

3.2. Nondetection of a reddened AGN in a submillimeter-bright object

Among the five known active nuclei in the 53W002 grouping, one is also identified as a submillimeter-bright source. Smail et al. (2003) have combined SCUBA mapping with VLA continuum data at 1.4 Ghz to identify object 18 of Pascarelle et al. (1996) with the submillimeter source, implying a bolometric luminosity of 8×10^{12} solar luminosities. The origin of this energy output is not clear; all the properties of this object observed in the

optical and near-IR are traceable to a luminous, largely obscured, active nucleus and its surrounding emission and reflection nebulae. This interpretation is strengthened by the *Chandra* spectrum, which shows a heavily absorbed power-law form (White et al. 2004). This object has an especially extensive Lyman α halo, whose ionization is most easily explained if our line of sight suffers unusually high extinction (so that the UV continuum that we do observe would be scattered light). The ISO nondetection of this object shows that any such luminous central source must be quite strongly obscured. It must be fainter than 53W002 itself at 6.7μm, which requires an emitted-frame color $V - K < 3.3$. Such a blue limit implies that any obscured nucleus does not yet dominate the light at 2μm. A typical QSO continuum must be reddened by $A_V > 1.2$ to have this color in $V - K$, and the reddening must be substantially greater in this case because the continuum at shorter wavelengths is quite blue (as shown by Keel et al. 2002) and thus cannot be reddened AGN light (although scattered light could play a role). The resolved continuum from NICMOS observations also indicates that little direct AGN light emerges in our direction in the $0.3 - 0.6\mu$m emitted range. Given the uncertainties in separating any direct starlight from side effects of the AGN, we can limit direct light from the AGN at these shorter wavelengths to less than about 20% of the total.

3.3. Narrow-Line Lyman α Star-Forming Objects

We set a mean limit on the 6.7μm flux of the faint blue Lyman α emitters in this field, by adding 20×20" regions around each of them registered on the optical positions. The objects stacked were numbers 5,11,12,29,34,60, and 113 from Pascarelle et al. (1996). Of these, 5 and 12 are at $z = 2.05$, 94 is at $z = 2.74$; and the rest are at $= 2.30 - 2.40$ (Pascarelle et al. 2004). This mean image gives a flux formally less than 0.010 mJy, slightly better than the noise statistics should allow. The 1σ noise level for 10" apertures

averaged over 7 objects gives 0.003 mJy, and the 5”-diameter effective apertures used for these unresolved objects would give group-mean 1σ levels close to 0.004 mJy. We therefore take the more conservative $3\sigma = 0.012$ mJy value, since the measured formal flux might be unusually low by small-number statistics. This means that on average they are at least three times fainter than 53W002 itself. The mean spectral slope can be evaluated against observed wavelengths near 1.6μm using NICMOS data (Keel et al. 2002), using the sample mean flux of 1.4×10^{-19} erg cm^{-2} s^{-1} Å^{-1}. The mean F_λ flux ratio between emitted wavelengths 0.47 and 2.0μm is then > 2.5, implying $V - K < 4.0$. This means that these objects could in principle have stellar populations as old, and formed over a span as long, as we infer for 53W002. A limit to dust emission from ongoing star formation can be set from the coadded SCUBA data, likewise stacked at the positions of these objects. The formal mean 850 μm flux is 0.14 ± 0.24 mJy. For objects with a spectral energy distribution like that of Arp 220, this flux (0.14 mJy) at $z = 2.4$ would correspond to a total far-IR luminosity $\approx 3 \times 10^{11}$ solar luminosities, or a mean star-formation rate of about 30 solar masses per year. This is a few times lower than implied by the typical mid-UV continua of these objects (using the star-formation form from equation 1 of Kennicutt 1998), which may attest to the nearly dust-free nature of the star-forming regions as seen in the very blue UV-optical colors (Keel et al. 2002).

In themselves, then, these data do not add to the case that the compact Lyman α emitters arise from short (perhaps repeated) bursts, either in small “protogalactic” systems (Pascarelle et al. 1996, 1998; Keel et al. 2002) or as pieces of larger systems whose typical surface brightness is below current detection thresholds (Colley et al. 1996).

4. Additional galaxy detections

Two lower-redshift galaxies are certain or probable detections at 6.7μm. The brightest, strong enough to be important in the astrometric registration of the data, is the merging system 53W003 at $z \sim 0.05$ (from the LBDS followup spectrum described by Windhorst, Kron, & Koo 1984). This system is a modest radio source as well (Windhorst, van Heerde, & Katgert 1984, from their table of additional sources). The detailed structure at 6.7μm is reproduced between two overlapping individual rasters, separating the northern and southern nuclei and showing the southern nucleus about twice as bright as the northern one. Convolved to similar resolution, both nuclei have similar $B - V$ and a flux ratio of about 1.4 (south/north). This object is identified with the IRAS faint-source survey object IRAS F17130+5021, with catalogued fluxes $F_{12} < 0.07$ Jy, $F_{25} < 0.08$ Jy, $F_{60} = 0.31$ Jy, and $F_{100} = 0.86$ Jy. This spectral shape is not particularly "hot" for a merging system, so it is either relatively quiescent in star formation or has not yet initiated a major starburst.

One fainter source, in the inner region of full exposure, has a likely counterpart in a spiral galaxy at $z = 0.3 - 0.6$, which appears in the WFPC2 images from Pascarelle et al. (1996). This spiral has two small, close, and blue companions. This is the optically brightest disk galaxy within the region of full ISO exposure. HST and ground-based images of these galaxies from B-K are shown in Fig. 5.

The optical and near-infrared magnitudes for these galaxies are listed in Table 2. We have estimated a redshift range for the faint spiral from its colors, using the K-correction calculations by Kinney et al. (1996).

One additional ISO source, slightly brighter than 53W002, falls near a faint galaxy (source number 7 in Fig. 3 and Table 1). This galaxy lies outside the WFPC2 and NICMOS observations of this region, so we have only ground-based broadband color data. Within a 3" aperture it has $B = 23.16$, $V = 21.75$, making it slightly brighter and significantly redder

than 53W002 itself (which has $V = 22.6$ and $B - V \approx 0.8$).

5. Mid-Infrared Source Counts

Source counts are of interest from any deep observation in newly-opened wavelength bands. The LW2 band around 6.7μm falls in an interesting spectral range. At low redshifts, this is on the long-wavelength, nearly Rayleigh-Jeans tail of emission from most stellar photospheres, so that only quite bright local galaxies (plus cool Galactic stars) will be prominent. At large redshifts, photospheric radiation shifts into this passband, making optically much fainter objects detectable. There will be a "valley" at moderate redshifts (from a few tenths to about $z = 2$) in which the only strong sources will be AGN, with flatter spectra sometimes augmented by hot dust. Since only a single ISO source appears to be associated with the targeted group at $z = 2.4$, we can use the others as a fair sample of the deep extragalactic sky. For the small solid angle covered, these counts serve largely as a sanity check on our reduction.

This region is part of the Herc 2 field surveyed in several passbands during the Leiden-Berkeley Deep Survey (LBDS; Windhorst, van Heerde, & Katgert 1984; Windhorst, Kron, & Koo 1984; Kron, Koo, & Windhorst 1985). The extinction is modest given the rather low galactic latitude $b = 35°$, with estimates from $A_B = 0.03$ from Burstein & Heiles (1984) to 0.09 (Schlegel et al. 1998). The far-IR cirrus emission and H I column density in this direction are similarly moderate for its latitude. Optical and radio source counts in this region reach very deep, with substantial numbers of photometric measurements and redshifts available.

Several additional deep studies were carried out using ISOCAM at 6.7μm, facilitating a comparison of source counts and populations. We compare here results from the HDF

observations of Oliver et al. (1997) and Serjeant et al. (1997), the HDF-S observations analyzed by Oliver et al. (2002), the ELAIS data presented by Serjeant et al. (2000), the SSA13 deep survey analyzed by Taniguchi et al. (2002) and Sato et al. (2003), the lens-amplified counts behind Abell 2390 from Altieri et al. (1999), and the Lockman Hole data from Taniguchi et al. (1997). Our coverage in solid angle is about 25500 arcsec^2 or 5.86×10^{-7} sr at full exposure, with the envelope of the entire area with any exposure spanning 89283 arcsec^2 or 2.05×10^{-6} sr. The strongest source, 53W003 at 7.0 mJy within a 15" radius, is brighter than would be expected in a random field based on the ELAIS+HDF counts at this wavelength from Serjeant et al. (2000), at about the 95% level. Counts of the fainter sources, limited as they are in number, are in reasonable agreement with the other surveys (Fig. 6).

We consider three subsamples of our source list. One subsample (labelled "ALL") consists of all except 53W002, which was the targeted object and should be omitted in constructing a random sample. The minimum list ("MIN") includes sources with optical identifications, which should be free of spurious IR souces at the expense of rejecting genuine sources which are very faint at shorter wavelengths. A further refined minimal extragalactic list ("XGAL") includes only those sources with nonstellar optical counterparts. Fig. 6 compares the highest and lowest of these with published counts, in the cumulative form, showing good agreement. In particular, the XGAL sample overlaps, within its error bounds, the ranges seen in the HDF, Abell 2390, and the Lockman Hole data, while the SSA 13 counts fall somewhat below all of these. This may fit with the radio-source counts; both the HDF-N and SSA13 are low compared to another ≈ 12 deep survey regions, in both cases connected to explicit field selection against strong radio sources (see Windhorst 2003). In retrospect, these higher counts are consistent with *Spitzer* counts transformed from the 5.8μm results reported by Fazio et al. (2004).

6. Conclusions

We have carried out a deep survey of the 53W002 galaxy group at $z = 2.4$, using ISO at roughly the emitted K band, to detect or limit any older stellar populations in the members and thus probe the onset of significant star formation. The radio galaxy 53W002 was detected at the 3σ level, giving emitted $V - K$ colors consistent with the earliest widespread star formation setting in at $z = 3.6 - 7.7$. The neighboring star-forming objects detected as narrow Lyman α emitters are so faint that even a group average flux limits provides a less stringent constraint than this; their emitted UV and implied composition give stronger constraints on their star-forming history at this point. The neighboring submillimeter-bright AGN is undetected in the ISO data, indicating that the direct continuum radiation from its active nucleus is quite heavily absorbed.

All these issues will be substantially clearer with the analysis of recent *Spitzer* observations by the IRAC team. These data should be able to narrow the onset of star formation in all these objects, and hence tell whether the more massive objects indeed began star formation earlier. These data might be able to test, at early times, the role of such issues as the upper asymptotic-giant branch in populations 0.2–1 Gyr old, whose potential importance in the near-IR bands has recently been stressed by Maraston (2004).

This work was supported by NASA through JPL contract 961525. We thank Dave van Buren for suggestions on observing strategies for achieving the best sensitivity. The ISOCAM data presented in this paper were analyzed using “CIA”, a joint development by the ESA Astrophysics Division and the ISOCAM Consortium. Stephan Ott and Babar Ali provided crucial assistance in setting up the ISOCAM analysis and in dealing with special problems that arose in processing these observations.

REFERENCES

Altieri, B., Metcalfe, L., Kneib, J.P., McBreen, B., Aussel, H., Biviano, A., Delaney, M., Elbaz, D., Leech, K., Lémonon, L., Okumua, K., Pelló, R., & Schulz, B. 1999, A&A, 343, L65

Blommaert, J., Siebenmorgen, R., Coulais, A., Okumura, K., Ott, S., Sauvage, M., & Starck, J.-L. 2001, ISO Handbook, volume III (CAM), version 1.2, section 4.11, ESA SAI/99-057/Doc, http://www.iso.vilspa.esa.es/manuals/HANDBOOK/III/

Burstein, D. & Heiles, C. 1984, ApJS, 54, 33

Cesarsky, C.J. et al. 1996, A&A, 513, L32

Colley, W. N., Rhoads, J. E., Ostriker, J. P., & Spergel, D. N. 1996, ApJ, 473, L63

Delaney, M., ed., 2000, ISOCAM Interactive Analysis User's Manual v4.0, ESA

Dunlop, J., Peacock, J., Spinrad, H., Dey, A., Jimenez, R., Stern, D., & Windhorst, R. 1996, Nature, 381, 581

Eales, S.A., & Rawlings, S. 1993, ApJ, 411, 67

Fazio, G.G. et al, 2004, ApJS (in press), astro-ph/0405595

Flores, H. et al. 1999, A&A, 343, 389

Hawarden, T.G., Leggett, S.K., Letawsky, M.B., Ballantyne, D.R. & Casali, M.M. 2001, MNRAS, 325, 563

Keel, W.C., Cohen, S., Windhorst, R.A., & Waddington, I. 1999, AJ, 118, 2547

Keel, W.C., Wu, W., Waddington, I., Windhorst, R.A., & Pascarelle, S.M. 2002, AJ, 123, 3041

Kennicutt, R. C. 1998, ARA&A, 36, 189

Kinney, A.L., Calzetti, D., Bohlin, R.C., McQuade, K., Storchi-Bergmann, T., & Schmitt, H.R. 1996, ApJ, 467, 38

Kron, R.G., Koo, D.C., & Windhorst, R.A. 1985, A&A 146, 38

Maraston, C. 2004, astro-ph/0402269

Monet, D.G. 1998, BAAS, 193, 120.03

Monet, D.G. et al. 2001, http://ftp.nofs.navy.mil/projects/pmm/USNOSA2doc.html

Motohara, K. et al. 2001, PASJ, 53, 459

Neuschafer, L.W. & Windhorst, R.A. 1995, ApJS, 96, 371

Oliver, S. et al. 1997, MNRAS, 289, 471

Oliver, S. et al. 2002, MNRAS, 332, 536

Osterbrock, D.E. 1989, Astrophysics of Gaseous Nebulae and Active Galactic Nuclei (MIll Vallye, CA: University Science Books)

Pascarelle, S.M., Windhorst, R.A., Keel, W.C., & Odewahn, S.C. 1996, Nature, 383, 45

Pascarelle, S.M., Windhorst, R.A. & Keel, W.C. 1998, AJ, 116, 2659

Pascarelle, S.M., Scoville, N.Z., Windhorst, R.A., & Cohen, S.H. 2004, ApJ, submitted

Pettini, M., Kellogg, M., Steidel, C.C., Dickinson, M., Adelberger, K.L., & Giavalisco, M. 1998, ApJ, 508, 539

Pettini, M., Shapley, A.E., Steidel, C.C., Cuby, J.-G., Dickinson, M., Moorwood, A.F.M., Adelberger, K.L., & Giavalisco, M. 2001, ApJ 554, 981

Sato, Y., Kawara, K., Cowie, L.L., Taniguchi, Y., Sanders, D.B., Matsuhara, H., Okuda, H., Wakamatsu, K., Sofue, Y., Joseph, R.D., & Matsumoto, T. 2003, A&A, submitted (astro-ph/0305120)

Schlegel, D.J., Finkbeiner, D.P., & Davis, M. 1998, ApJ, 500, 525

Scoville, N.Z., Yun, M.S., Windhorst, R.A., Keel, W.C., & Armus, L. 1997, ApJL, 485, L21

Serjeant, S.B.G. et al. 1997, MNRAS, 289, 457

Serjeant, S., et al. 2000, MNRAS, 316, 768

Smail, I., Ivison, R. J., Gilbank, D. G., Dunlop, J. S., Keel, W. C., Motohara, K., & Stevens, J. A. 2003, ApJ, 583, 551

Spinrad, H., Dey, A., Stern, D., Dunlop, J., Peacock, J., Jimenez, R., & Windhorst, R. 1997, ApJ, 484, 581

Stockton, A., Kellogg, M., & Ridgway, S. E. 1995, ApJ, 443, L69

Taniguchi, Y., Cowie, L.L., Sato, Y., Sanders, D.B., Kawara, K., Joseph, R., Okuda, H., Wynn-Williams, C.G., Matsumoto, T., Chambers, K.C., Wakamatsu, K., Désert, F.X., Sofue, Y., & Matsuhara, H. 1997, A&A, 328, L9

Taniguchi, Y. et al. 2001, in ASP Conf. Ser. 284, AGN Surveys, ed. R. F. Green, E. Ye. Khachikian, & D. B. Sanders (San Francisco: ASP), 32

Teplitz, H.I. et al. 2000, ApJ 542, 18

White, R.E., III., Keel, W.C., & Windhorst, R.A. 2004, ApJL (submitted)

Windhorst, R. A. 2003, in Proceedings of the Leiden/Lorentz Workshop on "High-Redshift Radio Galaxies — Past, Present and Future", Eds. M. J. Jarvis & H. J. A. Röttgering (Amsterdam: Elsevier), New Astron. Rev., Vol. 47, No. 4–5, 357

Windhorst, R. A., Gordon, J. M., Pascarelle, S. M., Schmidtke, P. C., Keel, W. C., Burkey, J. M., & Dunlop, J. S. 1994, ApJ, 435, 577

Windhorst, R.A., Keel, W.C. & Pascarelle, S.M. 1998, ApJL, 494, L27

Windhorst, R.A., Kron, R.G., & Koo, D.C. 1984, A&AS 58, 39

Windhorst, R.A., van Heerde, G.M., & Katgert, P. 1984, A&AS 58, 1

Windhorst, R. A., et al. 1991, ApJ, 380, 362

Worthey, G. 1994, ApJS, 95, 107

This manuscript was prepared with the AAS LaTeX macros v4.0.

ID	α_{2000}	δ_{2000}	F_ν, mJy	Notes
1	17:14:16.9	+50:18:16	6.5 ± 1.1	53W003
2	17:14:04.8	+50:17:22	0.080 ± 0.010	5" W of star
3	17:14:19.1	+50:17:20	0.069 ± 0.006	star
4	17:14:05.3	+50:15:17	0.069 ± 0.015	blank field
5	17:14:21.5	+50:16:17	0.057 ± 0.008	blank field
6	17:14:10.2	+50:16:08	0.045 ± 0.006	red star
7	17:14:17.2	+50:15:04	0.044 ± 0.006	faint galaxy?
8	17:14:15.2	+50:16:50	0.041 ± 0.005	red star or compact galaxy
9	17:14:12.8	+50:16:45	0.035 ± 0.006	spiral galaxy
10	17:14:14.8	+50:15:30	0.031 ± 0.007	53W002

Table 1: Source detections in LW2 field

Source	B	V	I	K	aperture	z_{phot}	Notes
1	15.85	14.78	...	...	32"	0.05	53W003
9	19.17	17.56	16.61	...	$4\rlap{.}''0$	0.3–0.6	

Table 2: Optical fluxes and redshifts for detected galaxies

Fig. 1.— Overlap pattern of individual LW2 rasters superimposed over a version of processed 6.7μm mosaic, in which no masking of raster borders was done so as to preserve the full field for this illustration and background variations have not been removed. The numbers denote observation sequence numbers; 931–947 are from orbit 500, while 703–729 were observed on orbit 521. The circled cross shows the location of 53W002. The low-redshift system 53W003 is prominent to the northeast (upper left).

Fig. 2.— Final mosaicked 6.7μm image of the 53W002 field, incorporating masking of the edges of individual rasters to reduce artifacts in the clipped mean and median filtering of sky variations though an 11×11" window. The rapid increase in noise to the edge of the mosaic, outside the central 90" radius, is still apparent. The maximum extent of the exposed region is 347" N-S and 354" E-W. The prominent elongated source at upper left is the low-redshift merging system 53W003.

Fig. 3.— Sources in the 53W002 field, as shown on a Gaussian-smoothed LW2 image (smoothed to 5" FWHM, left) and a blue-light image (right, with 4100-Ådata from Keel et al. 1999) resampled to the same scale. Sources listed in Table 1 are marked. Number 1 is 53W003, number 10 is at the position of 53W002 at $z = 2.39$.

Fig. 4.— The infrared spectral energy distribution of 53W002 compared to model stellar populations. The near-IR points, mapping to the emitted optical near the B and R bands, are the NICMOS and IRTF data from Keel et al. (2002) incorporating correction for the central AGN. The model stellar populations are from the Worthey (1994) code as implemented on the World-Wide Web. The error range for the ISO point spans ages of 1.0–2.0 Gyr, corresponding to redshifts at the onset of significant star formation $z_f = 3.6 - 7.0$ with a central value of $z_f = 4.7$.

Fig. 5.— Optical images of moderate-redshift galaxies with ISO 6.7μm detections. The

images of 53W003 are B and V KPNO 4m prime-focus data from Keel et al. (1999), since this systems falls outside our HST imagery. The southern nucleus of this apparently merging system is the peak of 6.7μm radiation. The area shown for 53W003 is 67 arcseconds square. For the spiral listed as ISO source 9, 10×10-arcsecond sections of WFPC2 images are shown in F450W (B), F606W (V), and F814W (I), from the observations described by Pascarelle et al. (1996). The B image is reconstructed from data taken using a 2×2 dither pattern so the pixel spacing is $0''.05$ rather than $0''.1$ as obtained from a single WFPC2 image (as for the V and I data). The brightness scale in each case is pseudologarithmic, using a flux offset of 1% of the maximum to avoid a discontinuity at the mean sky level. Each image has been rotated to place north at the top and east to the left.

Fig. 6.— Counts of ISO sources from deep observations at 6.7μm. Cumulative counts from our observations in the 53W002 field are shown for all sources and for those objects not optically identified with foreground stars (XGAL). The error bars are for Poisson statistics, except that the highest-flux point, above which there is a single detection, is shown with $\pm 50\%$ error bounds for clarity. The shaded region encompasses the $\pm 1\sigma$ bounds for the XGAL and all-detection sample. These overlap substantially with the counts reported for the HDF , Abell 2390, and Lockman Hole data, especially for the XGAL sample.

This figure "fig1.gif" is available in "gif" format from:

http://arXiv.org/ps/astro-ph/0406438v1

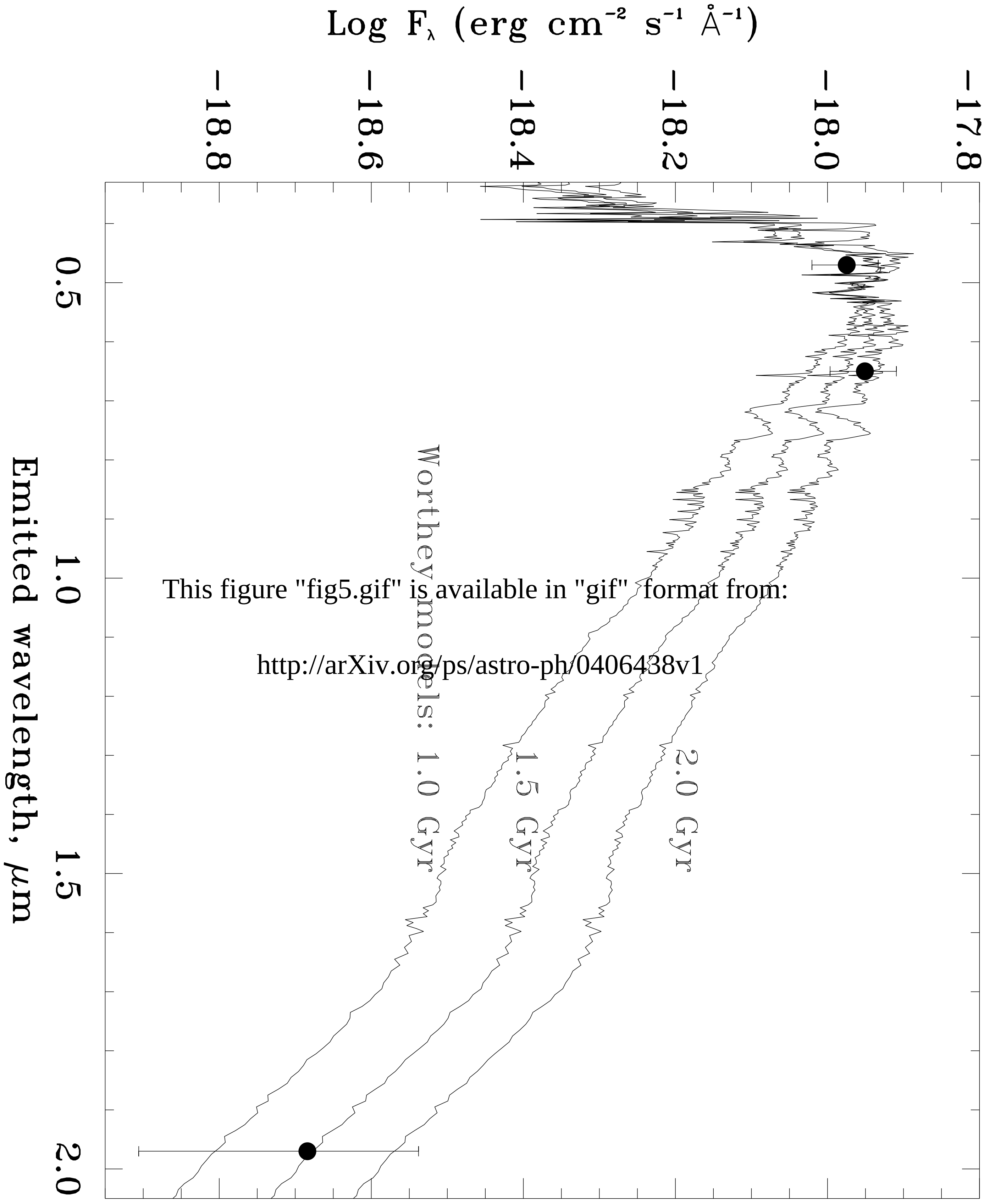
Log F$_\lambda$ (erg cm^{-2} s^{-1} Å^{-1})
−18.8
−18.6
−18.4
−18.2
−18.0
−17.8
0.5
1.0
1.5
2.0
Emitted wavelength, μm
Worthey models: 1.0 Gyr
1.5 Gyr
2.0 Gyr